Sensorless Drive for Salient Synchronous Motors based on Direct Fitting of Elliptical-Shape High-Frequency Currents

L. Ortombina, *Member*, *IEEE*, M. Berto, *Student Member*, *IEEE*, and L. Alberti, *Senior Member*, *IEEE*

Post Conference Paper

***Abstract*—The paper deals with a position sensorless control for synchronous motor drive with an ease tuning procedure and a reduced number of tunable parameters. The rotating high frequency (HF) signals injection is implemented and the elliptical shape of the HF induced current trace is fitted by means of the least square (LS) algorithm. The ellipse tilt is related to the rotor position and the latter is estimated by processing the fitted coefficients of the ellipse mathematical equation. The proposed LS algorithm processes the measured currents, without the need to filter them as occurs in conventional injection methods. Furthermore, no motor parameters are required to tune the proposed rotor position observer. The method was validated throughout several experimental tests performed on an interior permanent magnet (IPM) synchronous motor.**

***Index Terms*—ellipse fitting, high-frequency (HF) rotating injection, interior permanent magnet (IPM) motor, position observer, sensorless control, synchronous reluctance (SynR) motor**

I. Introduction

SYNCHRONOUS motors are widely adopted in applications where high dynamic performance and high efficiency are demanded. To achieve a satisfactory motor control, the accurate rotor position is required and is usually obtained by means of a mechanical sensor. However, the sensor and its cabling reduce the drive reliability and increase the system price and the motor frame. At standstill and in low speed region, fundamental signals are null or their signal-to-noise ratio is so small that ensuring a reliable estimate is troublesome. Observers based on fundamental components cannot be effectively exploited [1], [2]. Rotor position can be detected by processing the high frequency (HF) currents induced by HF voltage signals superimposed to the fundamental components, provided that the rotor anisotropy is detectable [3]–[5]. HF injection methods can be classified according to the reference frame in which HF signals are injected. HF voltage injection into the stator reference frame is usually referred to as *rotating signal injection* [4], [6]–[8]. Techniques that rely on a HF voltage signal injected in one of the estimated synchronous reference frame axis, usually the d–axis [3], [5], [9], [10], are named as *pulsating signal injection*.

Regardless of the reference frame chosen for HF voltage injection, position estimation algorithms are based on the modulation/demodulation theory, also known as heterodyne principle. Rotating signal injection schemes demodulate the negative–sequence carrier current through a synchronous reference filter [11] whereas pulsating injection techniques demodulate the measured HF pulsating current along the estimated q-axis [10]. The rotor position is retrieved by means of an observer which is fed by the demodulated signal. The modulation/demodulation stage has to be accurately described to design a proper observer which guarantees the desired performance. It is not a trivial task and it has been effectively carried out only for the pulsating signal injection scheme where the whole estimator was described and experimentally verified using exclusively the Laplace theory [3]. The heterodyne principle leads to a frequency shift of filters transfer function (TF) which is usually neglected by description methods which blend together time and Laplace-domain expressions.

An accurate estimator modelling allows for achieving the desired observer performance by means of a tailored observer regulator and for keeping the control bandwidth independent with respect to the motor working point [12]. The static gain of the observer, then the closed–loop observer bandwidth, varies as a function of motor inductances, thus motor parameters must be properly identified to compensate their variations [13]. Neglecting compensation or estimation errors, undesired dynamic behaviour of the observer, and sometimes, stability issues could arise. It is worth noting that motor saturation is more pronounced with Interior Permanent Magnet (IPM) and Synchronous Reluctance (SynR) motors which are inherently the most suitable motors for the HF rotor position estimation thanks to their high rotor anisotropy [14]. HF-based sensorless schemes are affected by an estimation error due to cross-differential inductance, which could heavy affect the control

This work has been developed in the frame of the "Green-seed" project funded by Italian Ministry of Research (MUR) within the call PRIN-2017 (Project 2017SW5MRC).

L. Ortombina, M. Berto and L. Alberti are with the Department of Industrial Engineering, University of Padova, Padova, 35131, Italy (e-mail: ludovico.ortombina@unipd.it, matteo.berto.2@phd.unipd.it, luigi.alberti@unipd.it). The corresponding author is Ludovico Ortombina.

performance. For a stable and reliable estimator behaviour, compensation techniques must be implemented [5], [15], [16].

The demodulation process recovers the baseband signal by shifting and filtering the spectrum of the measured currents. High pass filters (HPF)s extract the HF current components which are demodulated to get the baseband signal. In addition to the baseband signals, the demodulated signals contain sinusoidal terms at twice the modulation frequency which are usually removed thanks to a low pass filter (LPF) [4], [9], [10]. Moreover, when the rotating signal injection is implemented, a synchronous reference filter should be implemented to remove the positive–sequence carrier current [11]. The cut–off frequencies and the order of filters must be properly chosen as a trade–off between filtering effectiveness and invasiveness on the observer performance, which are opposing objectives. The thorny issue of filters tuning is partially overcome by square wave injection techniques which replace the conventional injected sinusoidal signal with a square wave one [17]–[19]. The high injection frequency makes it possible to simplify the demodulator by eliminating all filters except those that extract HF signals from the measured currents. On the other hand, the higher the injection frequency, the lower the signal-to-noise ratio of the HF components with respect to the measured currents, making accurate measurements crucial.

In this paper, a sensorless algorithm is proposed with the aim of overcoming the above mentioned critical issues related to the heterodyne-based sensorless techniques, namely, a precise observer modelling, an accurate motor parameter knowledge and the filters design. The rotating injection scheme is exploited and the rotor position is retrieved via a direct fitting of the measured current samples using the least square (LS) algorithm. The induced HF current footprint has an elliptical shape and its tilt is related to the rotor position [6], [7]. To ease the observer design and to enhance the observer dynamic with respect to [6], [7], required HPFs to centre the current ellipse on the axes origin are removed. It is worth stressing that the lack of filters has a twofold advantage, namely it simplifies the development of the estimation algorithm and makes its mathematical description smooth. The performance of the proposed sensorless algorithm is independent from the motor parameter knowledge in contrast to [4], [5], [9] since motor parameters only affect the current trace size, not its tilt which is related to the rotor position. An accurate machine identification is no longer required. Finally, the proposed estimator is time–domain defined thus its modelling is easier and the observer regulator tuning is straightforward.

This paper enlarges the theoretical and experimental results reported in [20]. An in-depth theoretical analysis, a comparison and more severe experimental results are reported. The paper is organised as follows. The theoretical background of the rotating injection sensorless technique is described in Section II. The proposed algorithm is thoroughly explained in Section III. The observer design is exhaustively discussed and a regulator scheme is described in Section IV. A complete set of experimental tests is reported in Section V, accompanied by an in-depth discussion of the results.

II. Theoretical background

A. Motor equations

The voltage balance equations of a synchronous motor in the stationary reference frame are:

$$\begin{aligned} u_\alpha &= R_s i_\alpha + \frac{d\lambda_\alpha(i_\alpha, i_\beta, \vartheta_{\mathrm{me}})}{dt} \\ u_\beta &= R_s i_\beta + \frac{d\lambda_\beta(i_\alpha, i_\beta, \vartheta_{\mathrm{me}})}{dt} \end{aligned} \tag{1}$$

where u_α, u_β are the stator voltages, i_α, i_β are the stator currents, λ_α and λ_β are the flux linkages, R_s is the stator resistance and $\vartheta_{\mathrm{me}} = p\vartheta_{\mathrm{m}}$ are electrical position, pole pairs and mechanical position, respectively. It is worth highlighting the explicit dependence of the flux linkages on the stator currents and on the rotor position in (1). The flux linkages can be described as a function of the apparent motor inductances L_α and L_β and the permanent magnet (PM) flux linkage Λ_{mg}, namely:

$$\begin{aligned} \lambda_\alpha(i_\alpha, i_\beta, \vartheta_{\mathrm{me}}) &= L_\alpha(i_\alpha, i_\beta, \vartheta_{\mathrm{me}}) i_\alpha + \Lambda_{\mathrm{mg}} \cos(\vartheta_{\mathrm{me}}) \\ \lambda_\beta(i_\alpha, i_\beta, \vartheta_{\mathrm{me}}) &= L_\beta(i_\alpha, i_\beta, \vartheta_{\mathrm{me}}) i_\beta + \Lambda_{\mathrm{mg}} \sin(\vartheta_{\mathrm{me}}). \end{aligned} \tag{2}$$

Replacing (2) in (1), the flux linkage derivatives with respect of time result:

$$\begin{aligned} \frac{d\lambda_\alpha}{dt} &= l_\alpha \frac{di_\alpha}{dt} + l_{\alpha\beta} \frac{di_\beta}{dt} + \omega_{\mathrm{me}} \left(\frac{dL_\alpha}{d\vartheta_{\mathrm{me}}} i_\alpha - \Lambda_{\mathrm{mg}} \sin(\vartheta_{\mathrm{me}}) \right) \\ \frac{d\lambda_\beta}{dt} &= l_{\alpha\beta} \frac{di_\alpha}{dt} + l_\beta \frac{di_\beta}{dt} + \omega_{\mathrm{me}} \left(\frac{dL_\beta}{d\vartheta_{\mathrm{me}}} i_\beta + \Lambda_{\mathrm{mg}} \cos(\vartheta_{\mathrm{me}}) \right) \end{aligned} \tag{3}$$

where l_α, l_β and $l_{\alpha\beta}$ are the differential motor inductances. To lighten the mathematical notation, the explicit stator currents and rotor position dependence have been hidden. In order to exploit the inductances properties of synchronous motors, differential inductances in the stationary reference frame can be rewritten as a function of the meaningful differential inductances l_{d}, l_{q} and l_{dq} defined in the *dq* rotating reference frame fixed to the rotor as follow:

$$\begin{aligned} l_\alpha &= l_\Sigma + l_\Delta \cos(2\vartheta_{\mathrm{me}}) - l_{\mathrm{dq}} \sin(2\vartheta_{\mathrm{me}}) \\ l_\beta &= l_\Sigma - l_\Delta \cos(2\vartheta_{\mathrm{me}}) + l_{\mathrm{dq}} \sin(2\vartheta_{\mathrm{me}}) \\ l_{\alpha\beta} &= l_\Delta \sin(2\vartheta_{\mathrm{me}}) + l_{\mathrm{dq}} \cos(2\vartheta_{\mathrm{me}}) \end{aligned} \tag{4}$$

where $l_\Sigma \triangleq (l_{\mathrm{d}} + l_{\mathrm{q}})/2$ is the *dq* differential inductance mean value and $l_\Delta \triangleq (l_{\mathrm{d}} - l_{\mathrm{q}})/2$ is the *dq* differential inductance semi-difference value. Still, differential inductances l_{d}, l_{q} and l_{dq} depend on the operating point as much as the flux linkages in (1).

B. Rotating voltage estimator

The rotating injection sensorless techniques retrieve the rotor position by injecting two HF sinusoidal voltage signals in the stationary reference, i.e.:

$$u_{h,\alpha} = U_{\mathrm{h}} \cos(\omega_{\mathrm{h}} t) \qquad u_{h,\beta} = U_{\mathrm{h}} \sin(\omega_{\mathrm{h}} t) \tag{5}$$

where U_{h} and ω_{h} are the magnitude and the pulsation of the injected sine waves. The HF signals (5) are superimposed to the fundamental voltage reference (U_α^*, U_β^*) generated

by current controllers. HF currents induced by the voltage injection are:

$$\begin{aligned} i_{h,\alpha} &= I_{\mathrm{s}}\Big(l_{\Sigma}\sin(\omega_{\mathrm{h}}t)+\sqrt{l_{\Delta}^2+l_{\mathrm{dq}}^2}\sin(2(\vartheta_{\mathrm{me}}-\bar{\vartheta})-\omega_{\mathrm{h}}t)\Big) \\ i_{h,\beta} &= -I_{\mathrm{s}}\Big(l_{\Sigma}\cos(\omega_{\mathrm{h}}t)+\sqrt{l_{\Delta}^2+l_{\mathrm{dq}}^2}\cos(2(\vartheta_{\mathrm{me}}-\bar{\vartheta})-\omega_{\mathrm{h}}t)\Big) \end{aligned} \tag{6}$$

where $I_{\mathrm{s}} \triangleq U_{\mathrm{h}}/(\omega_{\mathrm{h}}(l_{\mathrm{d}}l_{\mathrm{q}}-l_{\mathrm{dq}}^2))$ and $\bar{\vartheta} = 0.5\,\mathrm{atan2}(-l_{\mathrm{dq}}, l_{\Delta})$. At the injection frequency, the resistive voltage drop is negligible with respect to the inductive one, whereas the motional voltage terms are disregarded due to the low operating speed. The currents in (6) are composed of a positive–sequence component, rotating at the pulsation ω_{h}, and a negative–sequence one. The former contains no information about the rotor position whereas the latter one can be exploited to estimate the electromechanical rotor position. To retrieve the rotor position from the negative–sequence component of (6), heterodyne-based schemes isolate the desired current harmonics by means of filters. Hence, the spatial information contained in the phase of the negative–sequence component can be extracted by using a tracking observer.

The error signal ϵ which steers the rotor position observer can be obtained by demodulating the HF currents (6) as follow:

$$\begin{aligned} \epsilon &= i_{h,\alpha}\cos(-\omega_{\mathrm{h}}t+2\widehat{\vartheta}_{\mathrm{me}}) - i_{h,\beta}\sin(-\omega_{\mathrm{h}}t+2\widehat{\vartheta}_{\mathrm{me}}) \\ &= I_{\mathrm{s}}\sqrt{l_{\Delta}^2+l_{\mathrm{dq}}^2}\sin(2(\vartheta_{\mathrm{me}}-\widehat{\vartheta}_{\mathrm{me}}-\bar{\vartheta})) \\ &\approx 2I_{\mathrm{s}}\sqrt{l_{\Delta}^2+l_{\mathrm{dq}}^2}(\vartheta_{\mathrm{me}}-\widehat{\vartheta}_{\mathrm{me}}-\bar{\vartheta}) \end{aligned} \tag{7}$$

where $\widehat{\vartheta}_{\mathrm{me}}$ is the estimated rotor position and the sine function is approximated with its argument since a small estimation error is assumed. Finally, driving the demodulated signal (7) to zero by means of an observer, the rotor position is estimated and it can be exploited for the motor control. Let $\widetilde{\vartheta}_{\mathrm{me}} = \vartheta_{\mathrm{me}} - \widehat{\vartheta}_{\mathrm{me}}$ be the estimation error, it is worth noting that the stable point of the observer is affected by an estimation error $\widetilde{\vartheta}_{\mathrm{me}} = \bar{\vartheta}$. The observer is unable to accurately track the rotor position due to the non–zero cross–differential inductances l_{dq} since $l_{\mathrm{dq}} \neq 0$ entails $\bar{\vartheta} \neq 0$.

III. Ellipse Fitting

The proposed method retrieves the rotor position by exploiting the trajectory described by the HF induced currents in the stationary reference frame. HF currents in (6) describe an elliptical trajectory centered on the fundamental current vector (I_α, I_β) and rotates at the electrical motor speed ω_{me}. Its major axis tilt corresponds to the electrical rotor position. In order to retrieve it from the sampled currents, [6], [7] recursively fit the best ellipse curve centered on the axes origin over the sampled currents. Analogously to demodulation–based methods, at first the measured currents are filtered by means of a HPF to get a zero–centered ellipse. Then, the recursive least square (RLS) algorithm is used to estimate the ellipse equation coefficients that best fit the measurements. The approach in [7] is computationally efficient but its tuning is troublesome since the optimal forgetting factor in the RLS varies with the operating motor speed and it can be set only through a trial and error approach. Moreover, HPFs are not able to keep the ellipse trajectory centered on the origin during transients with a consequent worsening of the rotor position estimation.

The proposed method overcomes the above mentioned flaws by fitting the current footprint with the implicit ellipse equation, without high–pass filtering. The implicit ellipse equation is:

$$a i_\alpha^2 + b i_\alpha i_\beta + c i_\beta^2 + d i_\alpha + e i_\beta = f \tag{8}$$

where $\boldsymbol{\Theta} = [a, b, c, d, e, f]^T$ is the vector of coefficients that describes an ellipse in the $\alpha\beta$ reference frame. It is worth remembering that the $\alpha\beta$ currents in (8) are composed by both the fundamental currents (I_α, I_β) and the HF induced ones $(i_{h,\alpha}, i_{h,\beta})$. The relationship between ellipse coefficients $\boldsymbol{\Theta}$ and the motor parameters is as follows:

$$\begin{aligned} a &= l_\Sigma^2 + l_\Delta^2 + l_{\mathrm{dq}}^2 + 2l_\Sigma\sqrt{l_\Delta^2+l_{\mathrm{dq}}^2}\cos(2(\vartheta_{\mathrm{me}}-\bar{\vartheta})) \\ b &= 4l_\Sigma\sqrt{l_\Delta^2+l_{\mathrm{dq}}^2}\sin(2(\vartheta_{\mathrm{me}}-\bar{\vartheta})) \\ c &= l_\Sigma^2 + l_\Delta^2 + l_{\mathrm{dq}}^2 - 2l_\Sigma\sqrt{l_\Delta^2+l_{\mathrm{dq}}^2}\cos(2(\vartheta_{\mathrm{me}}-\bar{\vartheta})) \\ d &= -(2aI_\alpha + bI_\beta) \qquad e = -(2cI_\beta + bI_\alpha) \\ f &= \frac{U_{\mathrm{h}}^2}{\omega_{\mathrm{h}}^2} - aI_\alpha^2 - bI_\alpha I_\beta - cI_\beta^2 \\ &= \frac{U_{\mathrm{h}}^2}{\omega_{\mathrm{h}}^2} - (l_\Sigma^2 + l_\Delta^2 + l_{\mathrm{dq}}^2)I^2 - 2l_\Sigma\sqrt{l_\Delta^2+l_{\mathrm{dq}}^2}I^2\cos(2\bar{\vartheta}) \end{aligned} \tag{9}$$

where $I = \sqrt{I_\alpha^2 + I_\beta^2}$. See the Appendix for the proof. The coefficients $[a, b, c]$ are exclusively function of motor inductances and rotor position whereas $[d, e, f]$ also depend on fundamental currents. It is worth noting that the ellipse tilt and, in turns, the rotor position is independent to the HF currents magnitude and to the fundamental currents, provided the ellipse trace is detectable. Hence, the rotor position ϑ_{me} can be easily estimated by the ellipse coefficients $[a, b, c]$, as follow:

$$\vartheta_{\mathrm{me}} - \bar{\vartheta} = \frac{1}{2}\mathrm{atan}\frac{b}{a-c} \tag{10}$$

where the rotor position differs from the actual one by the angle $\bar{\vartheta}$, as in the demodulation–based estimation algorithms (see Section II-B). A HF current–based estimation algorithm suffers of the estimation error induced by the cross–differential inductance and it could lead to stability issues of the sensorless motor drive. To overcome this important flaw, some compensation methods have been proposed [5], [15] or the pulsating q-flux linkage can be demodulated to assure zero tracking error [9]. Nevertheless, an in-depth analysis and its compensation overcomes the purposes of this paper which describes a new position estimation technique. From now on, to ease the dissertation, the cross–differential inductance error $\bar{\vartheta}$ will be neglected, i.e. $l_{\mathrm{dq}} = 0$ is assumed.

A. Least Square Algorithm

The proposed position estimation technique exploits the least square (LS) algorithm to estimate the ellipse coefficients $\boldsymbol{\Theta}$ by minimising the sum of the squared distance between the measured currents and the fitting model. The LS algorithm

solves overdetermined systems, hence N consecutive current samples must be stored and processed together to find the ellipse coefficients. N consecutive time step of (8) can be rearranged in the matrix form as:

$$\boldsymbol{H}\boldsymbol{\Theta} = \boldsymbol{y} \tag{11}$$

where:

$$\boldsymbol{H} = \begin{bmatrix} i_{\alpha,1}^2 & i_{\alpha,1}i_{\beta,1} & i_{\beta,1}^2 & i_{\alpha,1} & i_{\beta,1} \\ i_{\alpha,2}^2 & i_{\alpha,2}i_{\beta,2} & i_{\beta,2}^2 & i_{\alpha,2} & i_{\beta,2} \\ \vdots & \vdots & \vdots & \vdots & \vdots \\ i_{\alpha,N}^2 & i_{\alpha,N}i_{\beta,N} & i_{\beta,N}^2 & i_{\alpha,N} & i_{\beta,N} \end{bmatrix} \quad \boldsymbol{y} = \begin{bmatrix} f_1 \\ f_2 \\ \vdots \\ f_N \end{bmatrix}. \tag{12}$$

The vector $\boldsymbol{y}$ is unknown since it is a function of motor inductances (see (9)). To ease the estimation process, (11) can be normalised with respect to $\boldsymbol{y} = f\boldsymbol{I}$ which is considered constant for the N stored current samples, since the small current control bandwidth of a sensorless drive does not allow for fast current variations. Hence, defining the new normalised vector of ellipse coefficients $\boldsymbol{\Theta}_N = \boldsymbol{\Theta}/f$, an its estimation can be obtained as follow:

$$\widehat{\boldsymbol{\Theta}}_N = \left(\boldsymbol{H}^{\boldsymbol{T}}\boldsymbol{H}\right)^{-1}\boldsymbol{H}^T\boldsymbol{I}. \tag{13}$$

The sign of the term f depends on the motor operating point since motor inductances saturate and fundamental current vector magnitude varies. The estimated vector $\widehat{\boldsymbol{\Theta}}_N$ sign is affected by the sign of f and, in turn, affects the rotor position estimation (10) with a π–offset if f sign would be negative. To overcome this issue, the normalised $[\widehat{a}, \widehat{c}]$ ellipse coefficients, i.e. $[\widehat{a}_N, \widehat{c}_N] = [\widehat{a}, \widehat{c}]/\widehat{f}$, must be ensured positive, hence:

$$\text{if } (\widehat{a}_N < 0) \quad \text{then} \quad \widehat{\boldsymbol{\Theta}}_N = -\widehat{\boldsymbol{\Theta}}_N \tag{14}$$

as $[\widehat{a}_N, \widehat{c}_N]$ are always concordant. Finally, it is worth noting that the rotor position can be retrieved by using the estimated vector $\widehat{\boldsymbol{\Theta}}_N$ since (10) is not affected by the normalisation process.

The LS algorithm solves the overdetermined problem stated in (11). To guarantee an accurate coefficients estimation, the number of stored consecutive current samples processed by the LS algorithm plays a crucial role and it has to be chosen carefully as a trade–off between several requirements. First of all, the stored samples number N must ensure that the underlying problem (11) is, at least, a determined problem, i.e. N must be equal to or greater than the number of unknown parameters. Moreover, the more points are saved, the greater the available current footprint on which to fit the ellipse coefficients and the smaller the effects due to measurement noise. On the contrary, if the rotor is moving, the stored samples belong to several ellipse trajectories. The equation (8) describes a fixed ellipse in the stationary reference frame and it is related to a static position. It cannot take into account a rotor movement, hence the rotor position estimation accuracy may deteriorate. This issue will be addressed in Section III-B and a compensation method will be proposed. Finally, a large number of stored samples increases the computational burden demanded to estimate the rotor position and may pose some implementation issues on a real–time control board. As a rule of thumb, the number of stored samples N can be chosen as the maximum between the number of normalised ellipse coefficients, i.e. 5, and the rounded towards infinity of the ratio between the sampling frequency f_s and the injection frequency $f_\mathrm{h} = \omega_\mathrm{h}/(2\pi)$. It is worth noting that the latter condition allows for describing an entire ellipse trajectory.

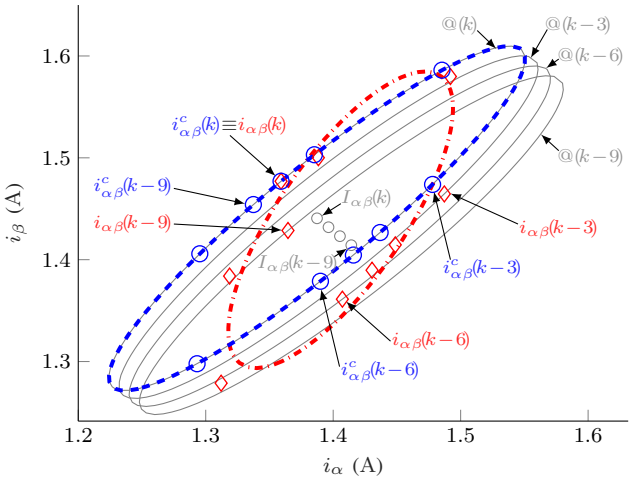

Fig. 1: The non–zero speed effect on the ellipse trajectory and the compensation method are depicted. Diamonds show ten consecutive $i_{\alpha\beta}$ current samples, each of which lies on a different ellipse corresponding to a rotor position. $i^c_{\alpha\beta}$ shows the compensated measured currents. The dashed blue and red trajectories depict the estimated ellipses by fitting the compensated samples and the measured ones, respectively.

B. Compensation of ellipse distortion due to non-zero speed

At standstill, the HF currents (6) draw a tilted ellipse in the $\alpha\beta$ reference frame. It can be fitted with the implicit ellipse equation (8) by means of the LS algorithm described in Section III-A and the rotor position is recovered. However, when the motor is running, the stored current samples belong to several ellipse trajectories, each describing a different rotor position. The ellipse equation (8) is not able to properly describe the actual current footprint and the estimation accuracy degrades. It downgrades more and more as the rotor speed increases and this flaw is more emphasised when a large number of current samples are stored. It worth remembering that injection–based sensorless techniques operate in the low speed region and, considering the high frequency of the injected voltage signals, this issue has a marginal effect. However, it can be effectively compensated for reducing its detrimental effect on the motor control.

The proposed compensation method updates the N consecutive stored current samples to the actual rotor position by assuming a constant motor speed. The n-th current sample is forward rotated in the stator reference frame by the electric angle that the motor has swept in $(n-1)$ sampling time T_s, namely:

$$\begin{aligned} i^c_{\alpha,n} &= i_{\alpha,n}\cos\left((n-1)\widehat{\omega}_\mathrm{me}T_s\right) - i_{\beta,n}\sin\left((n-1)\widehat{\omega}_\mathrm{me}T_s\right) \\ i^c_{\beta,n} &= i_{\alpha,n}\sin\left((n-1)\widehat{\omega}_\mathrm{me}T_s\right) + i_{\beta,n}\cos\left((n-1)\widehat{\omega}_\mathrm{me}T_s\right) \end{aligned} \tag{15}$$

where $i^c_{\alpha,n}$ and $i^c_{\beta,n}$ are the compensated current samples and $n \in [0, N-1]$. A smaller n-index indicates a newer sampled current. Fig. 1 shows an example of the proposed compensation method that was carried out at $\omega_{\rm me} = 20\pi\,{\rm rad/s}$. The fundamental current vector was $I_{\alpha\beta} = 2\,{\rm A}$ and the electrical rotor position was set to $\vartheta_{\rm me}(k) = 0.8042\,{\rm rad}$. Diamond marks represent $N = 10$ consecutive current samples which describe an entire ellipse curve. Each mark belongs to a different rotor position, represented with the corresponding grey ellipse. The center of each ellipse is depicted as well. To make the figure more readable, only four ellipses associated to four rotor positions are drawn. The estimated ellipse with the measured samples is shown with the dash-dotted line. Its tilt and its shape are misaligned with respect to the actual grey curves, which leads to a rotor position estimation $\widehat{\vartheta}_{\rm me} = 1.0887\,{\rm rad}$ that corresponds to an error of $\widetilde{\vartheta}_{\rm me} = -0.2845\,{\rm rad}$.

The ellipse distortion due to a non-zero rotor speed induces a considerable estimation error. The proposed compensation method perfectly estimates the rotor position, as depicted in Fig. 1. Circle marks show the compensated current samples $i^c_{\alpha\beta}$ with (15) and the dashed line is the fitted ellipse on $i^c_{\alpha\beta}$ points. All marks lie on the ellipse curve associated to the most recent rotor position and the fitted curve is overlapped to it. The estimated rotor position is coincident with the real one, i.e. $\widehat{\vartheta}_{\rm me}(k) = 0.8042\,{\rm rad}$. Hence, the updated current samples $i^c_{\alpha\beta}$ can replace the actual measurement $i_{\alpha\beta}$ in the LS matrices to obtain an error–free rotor position estimation. Finally, it is worth highlighting that the compensation strategy is based on a steady-state assumption, but is also applied during transients. The underlying hypotheses can still be assumed due to the reduced control bandwidth of sensorless schemes which do not allow fast transients and the low operating speeds.

C. Additional estimator feature

1) Ellipse centre estimation: The proposed algorithm processes the measured currents without any filtering. The elliptical trajectory due to the HF currents is centred in the fundamental current vector (I_α, I_β) in the stationary reference frame. The fitting equation (8) fully describes the current footprint and the ellipse centre can be retrieved by the fitted ellipse coefficients $\widehat{\boldsymbol{\Theta}}_N$, as follow:

$$\widehat{I}_\alpha = \frac{\widehat{b}\widehat{e} - 2\widehat{c}\widehat{d}}{4\widehat{a}\widehat{c} - \widehat{b}^2} \qquad \widehat{I}_\beta = \frac{\widehat{b}\widehat{d} - 2\widehat{a}\widehat{e}}{4\widehat{a}\widehat{c} - \widehat{b}^2} \tag{16}$$

where $(\widehat{I}_\alpha, \widehat{I}_\beta)$ is the estimated ellipse centre.

2) Measurement errors sensitivity analysis: Sensitivity analysis with respect to current measurement errors, namely, offset, gain and quantisation errors, is carried out. Only current sensor gain mismatches can lead to a relevant estimation error since the ellipse tilt, its shape and its center are affected. For large gain mismatches, the anisotropy of the rotor may even disappear. However, sensors are usually designed to show a linear and constant behaviour in the entire measurement range. Offset errors affect only the ellipse center, then position estimation is insensible. Finally, the proposed algorithm is robust against quantisation errors. Quantisation error can be modelled as a random quantity added on ideal current values, so the LS algorithm by simultaneously processing N current samples is able to extract their mean value, neglecting it.

IV. Regulator tuning

In conventional sensorless drives, the position estimator performance relies on the observer tuning, which has to ensure a fast and stable position estimation and a high disturbance rejection capability [3]. An accurate motor magnetic model is mandatory to tune the observer regulator and to achieve satisfactory performance of the sensorless drive.

The proposed method overcomes this flaw and it no requires the motor parameters knowledge. The ellipse fitting only processes the measured currents and estimate the best elliptical trajectory on the available data, without any tunable parameter. Nevertheless, the rotor position estimation with (10) only varies in the range $[0, \pi]$ due to the ellipse symmetry over π radian. It is a noisy estimation since is obtained by means of a trigonometric function with an estimated coefficients ratio as argument. In order to retrieve a smoother and in the proper range $[0,\, 2\pi]$ rotor position estimation, the sine and cosine of the estimated electrical position can be computed starting from the ellipse coefficients $\widehat{\boldsymbol{\Theta}}$, as follow:

$$\cos(2\widehat{\vartheta}_{\rm me}) = \frac{\widehat{a} - \widehat{c}}{\sqrt{\widehat{b}^2 + (\widehat{a} - \widehat{c})^2}} \qquad \sin(2\widehat{\vartheta}_{\rm me}) = \frac{\widehat{b}}{\sqrt{\widehat{b}^2 + (\widehat{a} - \widehat{c})^2}} \tag{17}$$

which feed a quadrature-PLL (Q-PLL), shown in Fig. 2. It recovers the rotor position $\widehat{\vartheta}_{\rm me}$ from the trigonometric functions and acts as a low–pass filter smoothing the estimation. Detrimental effects due to electrical drive non-idealities and current harmonics are kept at bay. A trade off between a smoother estimate and the closed–loop observer bandwidth must be met.

The relationship between the estimated rotor position $\widehat{\vartheta}_{\rm me}$ by means of the LS algorithm and the PLL output, namely $\widehat{\vartheta}'_{\rm me}$, is a constant unitary gain due to the fact that the PLL input vector, namely the sine and cosine components of the estimated rotor position, has a constant unitary amplitude. Compared to the classical demodulation approaches, no motor parameters affect the Q-PLL dynamic and its input–output transfer function $W({\rm s})$ is:

$$W({\rm s}) = \frac{\widehat{\vartheta}'_{\rm me}({\rm s})}{\widehat{\vartheta}_{\rm me}({\rm s})} = \frac{{\rm REG(s)}}{{\rm s} + {\rm REG(s)}} \tag{18}$$

where s is the Laplace variable and REG(s) stands for the Q-PLL regulator. If a proportional–integral controller is chosen as the regulator, its parameters can be set to place the closed–loop poles to achieve a critical damping factor $\xi_{\rm pll} = 1/\sqrt{2}$ and a desired natural pulsation $\omega_{\rm pll}$. To meet the aforementioned requirement, the proportional $K_{\rm p}$ and integral $K_{\rm i}$ can be chosen as:

$$K_{\rm p} = \sqrt{2}\omega_{\rm pll} \qquad K_{\rm i} = \omega^2_{\rm pll}. \tag{19}$$

From now on, to ease the notation, the Q-PLL output $\widehat{\vartheta}'_{\rm me}$ will be marked without the single quote mark, i.e. $\widehat{\vartheta}_{\rm me}$. Fig. 3 depicts the whole proposed sensorless control scheme.

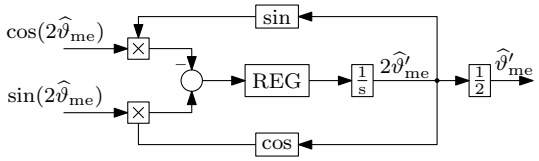

Fig. 2: Quadrature–PLL scheme.

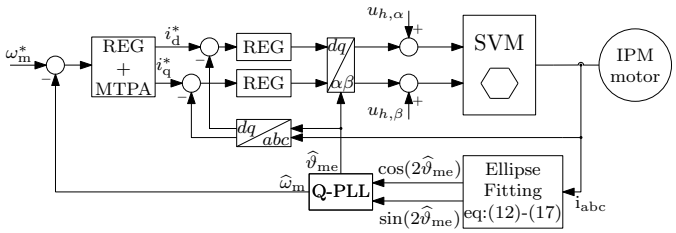

Fig. 3: Proposed sensorless control scheme.

V. Experimental results and discussion

The proposed position estimator algorithm was verified throughout an extensive experimental stage. The tests were performed on an IPM motor, whose parameters are reported in Table I. The injection signal quantities are listed in Table II. Current controllers were designed to achieve a bandwidth of 100 Hz. The sampling frequency was set equal to the switching one at 10 kHz and inverter dead-time was compensated [21]. The current samples number N was set to 10 as it allows describing an entire ellipse revolution. The algorithm was implemented on a dSpace MicroLabBox platform. The execution time of the whole electric drive control algorithm, including the estimation method, current and speed regulators, and space vector modulation, was equal to 27.5 µs for the proposed algorithm, whereas it was equal to 23 µs for the comparative method [4]. In the following, all the results are expressed in *per unit* (p.u.) quantity. Current, speed and torque are normalised with respect to their nominal values.

In order to prove the effectiveness of the proposed sensorless control, three different bunch of tests were carried out. The first tests were aimed at verifying the algorithm that compensates the ellipse distortion due to a non-zero speed and the estimation of the ellipse centre. These tests are reported in Section V-A and Section V-B, respectively. A second bunch of tests were designed to verify the dynamic performance of the proposed sensorless algorithm, during speed and load transient, and they are reported in Section V-C. Finally, the comparison with a demodulation–based scheme [4] is reported in Section V-D. In all experimental test, the motor under test was speed controlled and both current and speed loops used the estimated quantities. The active load was torque controlled.

A. Ellipse distortion compensation

A non-zero rotor speed spreads the N sampled current points over a trajectory which does not describe an ellipse with detrimental effects on the rotor position estimation. The trajectory distortion is increasingly pronounced as the rotor speed and the magnitude of the current vector increase. In order to prove the effectiveness of the proposed compensation

TABLE I: Plate data of the motor under test

Parameter	Symbol	IPM
Resistance	R_s	1.5 Ω
Pole pairs	p	2
d-axis inductance	l_d	25 mH
q-axis inductance	l_q	110 mH
Permanent magnet	Λ_mg	0.145 V s
Nominal current	I_N	3.9 A
Nominal torque	T_N	2.4 N m
Nominal speed	ω_N	4000 rpm

TABLE II: Sensorless parameters

Parameter	Symbol	
Injection pulsation	ω_h	$2\pi 1\,000$ rad/s
Injection magnitude	U_h	60 V

algorithm described in Section III-B, a test was carried out in the most critical conditions, namely high speed and rated torque. It is worth noting that the speed was set to 10% of the rated motor speed since it is considered the maximum speed at which injection-based schemes operate.

Fig. 4 depicts two sequences of consecutive measured current samples obtained with a time delay of 6 sampling periods. Full diamonds are common current samples in both subfigures. Despite the 10 measured samples should describe an entire ellipse rotation, an arc of ellipse can be grasped in Fig. 4a whereas the measured samples resemble an italic letter c in Fig. 4b. This current footprint distortion is due to a non-zero rotor speed, as each sample belongs to an elliptical trajectory relative to a different rotor position. Thus, position estimation is affected with detrimental effects. The tilt of the dash dotted estimated ellipse in Fig. 4a differs considerably from the one in Fig. 4b even if the rotor position is almost unchanged (the time span between the two current sequences is 0.6 ms, corresponding to $37.7\cdot10^{-3}$radel). This estimation error leads to a position estimate that periodically varies around the actual value and it can be noticed in Fig. 5 where the compensation algorithm is disabled. With the compensation method disabled, the estimation error considerably oscillates and a constant offset appears.

The proposed algorithm compensates the speed–distortion

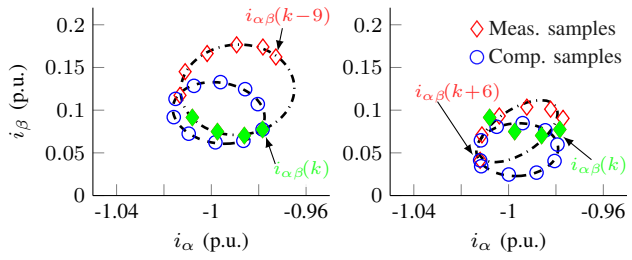

(a) Time instant 1 (b) Time instant 2

Fig. 4: Two sequences of 10 current samples spaced by 6 sampling periods. Compensated samples are reported, as well. Full diamonds are common samples in both time instants. Dot-dashed and dashed trajectories show the estimated ellipses.

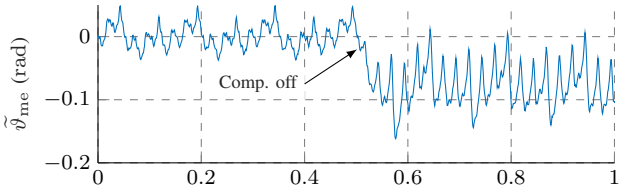

(a) Position estimation error

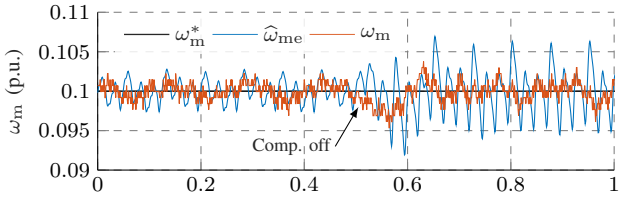

(b) Speed

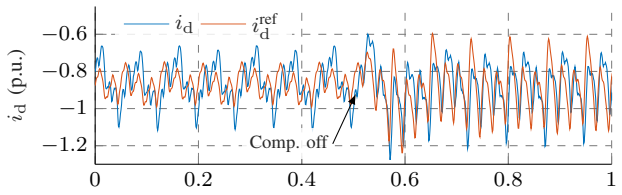

(c) *d*-axis current

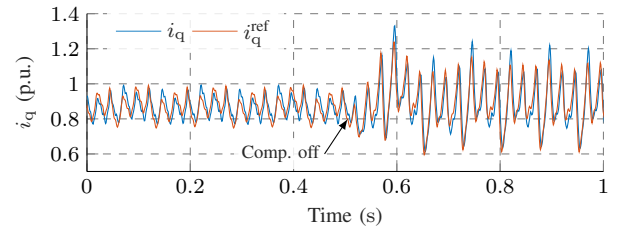

(d) *q*-axis current

Fig. 5: Proving of the compensation algorithm effectiveness. At t=0.5 s, the compensation algorithm was disabled. Position estimation error, motor speed and stator currents are reported, as well.

effect on the measured current samples. In both subfigures of Fig. 4, compensated samples describe an entire elliptical trajectory and points are well approximated by the fitted dashed curve. Moreover, in both Fig. 4a and Fig. 4b the fitted ellipses tilt are very close as expected, while the non–compensated ellipses tilts are quite different. Its consequence is a more accurate and less oscillating rotor position estimation, as Fig. 5 depicts. It is worth noting that a more precise position estimation positively affects both the estimated motor speed (Fig. 5b) and the motor currents (Fig. 5c and Fig. 5d) and, in turn, the overall electric drive performance.

B. Fundamental Current Estimation - Ellipse Centre

The proposed algorithm estimates the ellipse centre (I_α, I_β) with respect to [6], [7] as well as the rotor position. Fig. 6 depicts the first two electrical periods of measured currents recorded during the test described in Section V-A. They are almost sinusoidal waves as the motor is rotating at $10\%\omega_N$, but with some additional harmonics. Superimposed to fundamental

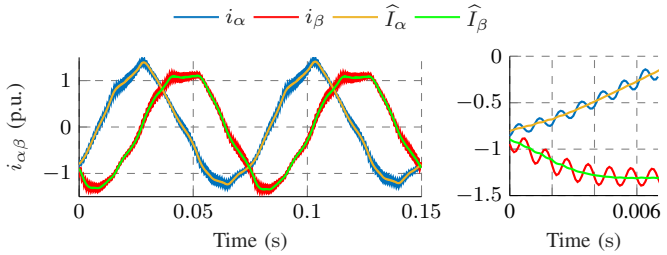

Fig. 6: Measured stator currents and fundamental estimated ones. An enlargement of the initial period is shown, as well.

components, there are the induced HF currents. The estimated fundamental currents $(\widehat{I}_\alpha, \widehat{I}_\beta)$ track with a good accuracy the measured currents regardless of current harmonics, filtering out the oscillating components without a phase lag.

C. Dynamic Performance Assessment

In this section, system performance was evaluated by means of two tests (see Fig. 7), performed at standstill and at 10% of the rated motor speed. In the non-zero speed case, the speed reference varied as a 0.1-second ramp to reach the steady state value. Moreover, to evaluate the control capability of reversing the motor speed, the speed reference was changed according to a 0.1-second slope ramp at t=2 s. Fig. 7a reports measured and estimated motor speed for both tests, as well as the speed reference. In both tests, a load torque double than the rated one was applied to the motor with a ramp of 0.05 second at 1 s. The measured torque is depicted in Fig. 7b for both tests. The discrepancy in measured torque according to speed sign has to be attributed to the viscous friction. The generated torque must balance the active load torque, which is constant, and the viscous friction one, which varies accordingly to the motor speed. The performance is evaluated by means of the position estimation error $\tilde{\vartheta}_{\mathrm{me}}$, shown in Fig. 7c. Finally, *d*- and *q*-currents are reported in Fig. 7d and Fig. 7e, respectively.

The dynamic performance of the proposed sensorless scheme is satisfactory, both at zero and low motor speed. Fast speed reference and load torque transients were applied to the motor. Motor speed properly followed its reference and stator currents shown no undesirable oscillation. The position estimation error is always smaller than 0.25 rad, even during transients. At twice the rated load, the estimation position error was almost negligible as it is equal to $\tilde{\vartheta}_{\mathrm{me}} = -0.023$ rad, as the chosen motor shows a reduced cross–differential inductance l_{dq}. By computing the position error $\bar{\vartheta}$ due to motor saturation at the operating point, it is equal to $\bar{\vartheta} = -0.028$ rad which is comparable to the obtained experimental error.

D. Method comparison

The performance comparison with an heterodyne–based estimator scheme [4] is hereafter reported. Fig. 8 shows two tests with a speed and torque reference profile equal to the one used in Section V-C. To get a fair comparison, speed and current regulators were unaltered in both tests and observers were tuned to achieve the same bandwidth. Measured speeds

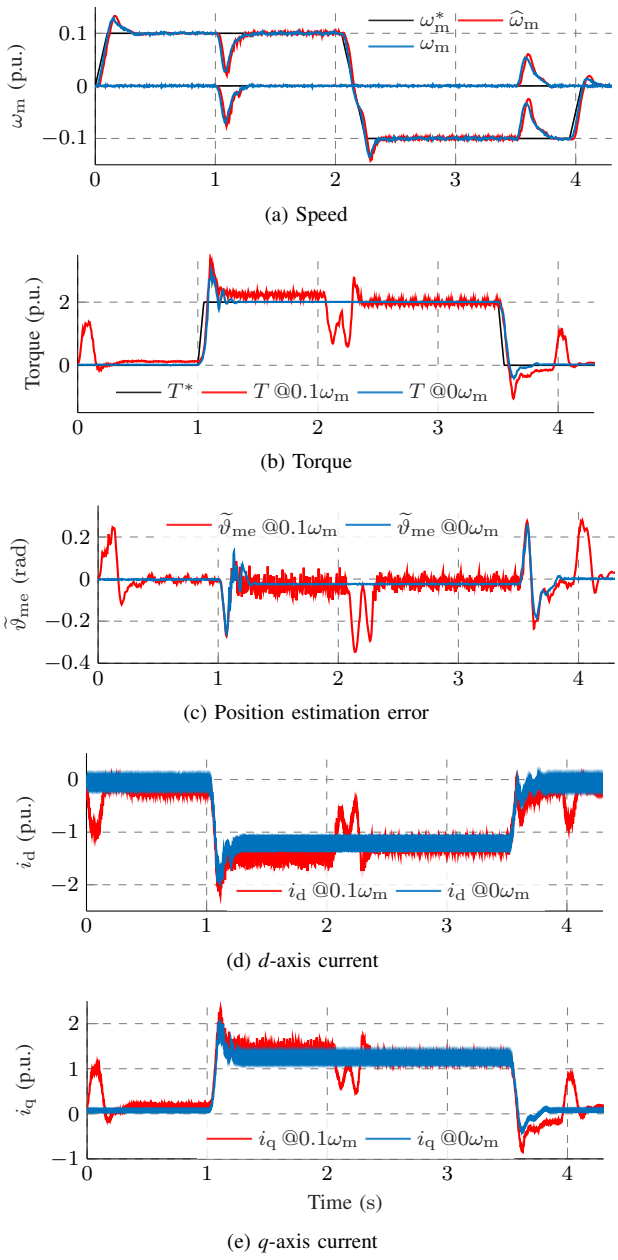

(a) Speed

(b) Torque

(c) Position estimation error

(d) *d*-axis current

(e) *q*-axis current

Fig. 7: Speed, torque, position estimation error and stator currents of dynamic tests. Two tests are reported with two different operating speeds.

and torques are depicted in Fig. 8a and Fig. 8b, respectively. The proposed method shown a slightly faster behaviour. Speed tracked its reference with a higher accuracy and speed response to load disturbance was faster. Moreover, it is worth noting that when the load was released and the speed reference was returned to zero, the proposed method exhibited a smooth behaviour whereas the other one showed an oscillating trend, which implies that some instability problem was arising. The oscillating behaviour could be further noted in the estimation error and in stator currents, which are reported in Fig. 8c, Fig. 8d and Fig. 8e. Finally, the integral time square error (ITSE), defined in (20), of the estimation position error for both method is reported in Fig. 8f.

$$\mathrm{ITSE} = \int_0^t \widetilde{\vartheta}_{\mathrm{me}}^2(t)dt \tag{20}$$

The proposed scheme outperformed the other method in terms of dynamic performance and in the ITSE-sense.

VI. Conclusions

The paper reports a novel rotor position estimation algorithm based on the rotating signal injection scheme. Neither HPF nor LPF are necessary in the observer algorithm. The induced HF currents trace an elliptical trajectory centred on the fundamental current vector. The HF current footprint is fitted on the implicit ellipse equation by means of the LS algorithm and the rotor position is directly retrieved. The rotor position or its sine and cosine components are computed by manipulating the estimated ellipse coefficients. A compensation method is proposed to improve the rotor position estimation since a non-zero rotor speed bends the theoretical HF current elliptical footprint. Finally, a Q-PLL is implemented to filter the estimated rotor position. Its design was thoroughly discussed and a tuning procedure was proposed. The main advantages compared to heterodyne-based methods are:

- Estimator dynamic easy to describe, as it is defined entirely in time–domain. Modelling issues related to the modulation/demodulation process are overcome. In turns, an accurate modelling helps to design a more effective speed regulator.
- Estimator open–loop gain is insensible to motor parameters. This advantage is useful when considering general–purpose applications, where the motor connected to the inverter is unknown and self–commissioning techniques are usually required.
- It is easy to implement and tune.

An extensive experimental stage was carried out to verify the performance of the proposed sensorless control, both at standstill condition and at no-zero speed. The sensorless drive was able to operate at the rated motor torque.

Appendix

The HF currents (6) can be rearranged to get the modulated signals $z_{\mathrm{c}} = \cos(\omega_{\mathrm{h}}t - \vartheta_{\mathrm{me}})$ and $z_{\mathrm{s}} = \sin(\omega_{\mathrm{h}}t - \vartheta_{\mathrm{me}})$ as:

$$\begin{aligned} z_{\mathrm{c}} &= \frac{\omega_{\mathrm{h}}}{U_{\mathrm{h}}}\big((l_{\mathrm{q}}\sin(\vartheta_{\mathrm{me}}) - l_{\mathrm{dq}}\cos(\vartheta_{\mathrm{me}}))i_{h,\alpha} - \\ &\qquad ((l_{\mathrm{q}}\cos(\vartheta_{\mathrm{me}}) + l_{\mathrm{dq}}\sin(\vartheta_{\mathrm{me}}))i_{h,\beta}\big) \\ z_{\mathrm{s}} &= \frac{\omega_{\mathrm{h}}}{U_{\mathrm{h}}}\big((l_{\mathrm{d}}\cos(\vartheta_{\mathrm{me}}) - l_{\mathrm{dq}}\sin(\vartheta_{\mathrm{me}}))i_{h,\alpha} + \\ &\qquad ((l_{\mathrm{d}}\sin(\vartheta_{\mathrm{me}}) + l_{\mathrm{dq}}\cos(\vartheta_{\mathrm{me}}))i_{h,\beta}\big). \end{aligned} \tag{21}$$

The HF currents can be rewritten as the difference between the measured currents (i_α, i_β) and their mean value (I_α, I_β) as:

$$i_{h,\alpha} = i_\alpha - I_\alpha \qquad i_{h,\beta} = i_\beta - I_\beta. \tag{22}$$

Replacing (22) in (21) and exploiting the Pythagorean identity $z_{\mathrm{c}}^2 + z_{\mathrm{s}}^2 = 1$, the ellipse coefficients (9) are collected by comparing the obtained equation with the ellipse one (8).

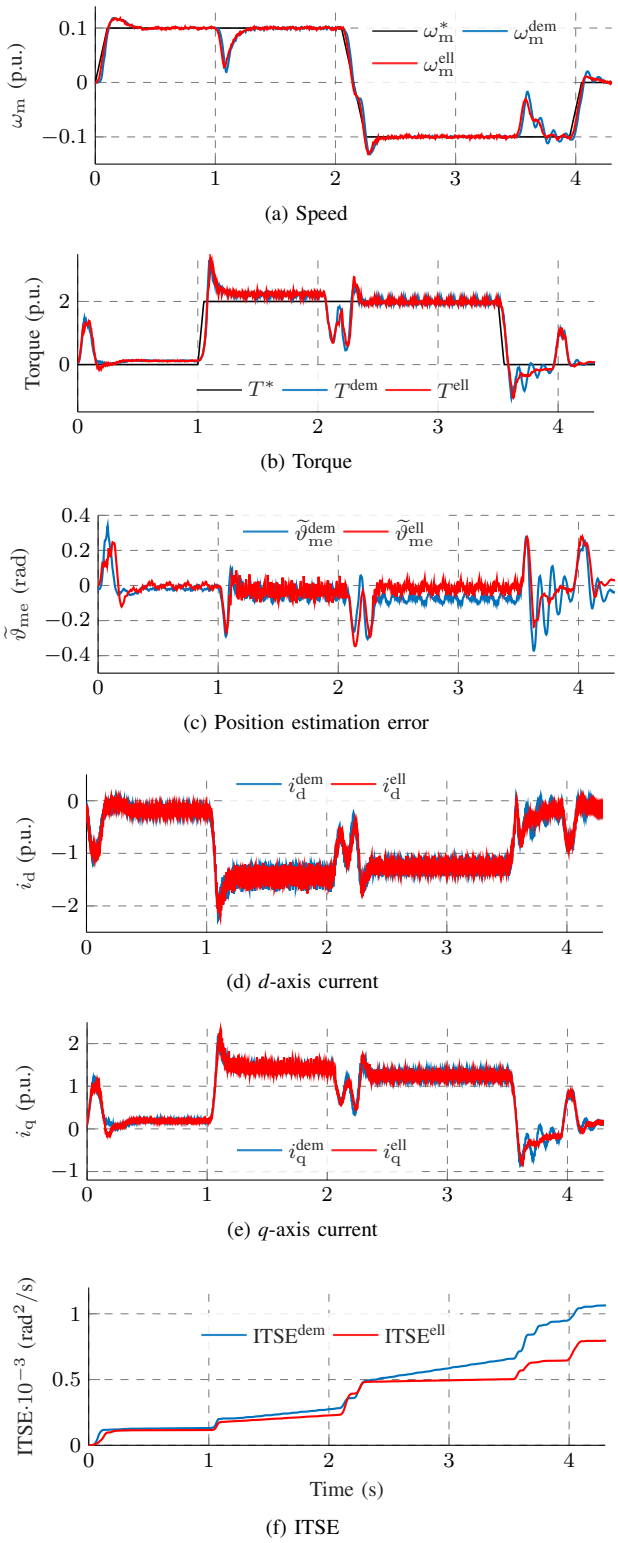

(a) Speed

(b) Torque

(c) Position estimation error

(d) d-axis current

(e) q-axis current

(f) ITSE

Fig. 8: Speed, torque, position estimation error, stator currents and ITSE index of a comparison test are reported. Proposed method is compared with an heterodyne-based one.

References

[1] Z. Chen, M. Tomita, S. Doki, and S. Okuma, "An extended electromotive force model for sensorless control of interior permanent-magnet synchronous motors," *IEEE Trans. Ind. Electron.*, vol. 50, no. 2, pp. 288–295, 2003.

[2] I. Boldea, M. C. Paicu, and G. Andreescu, "Active flux concept for motion-sensorless unified AC drives," *IEEE Trans. Ind. Electron.*, vol. 23, no. 5, pp. 2612–2618, 2008.

[3] L. Ortombina, D. Pasqualotto, F. Tinazzi, and M. Zigliotto, "Comprehensive analysis and design of a pulsating signal injection-based position observer for sensorless synchronous motor drives," *IEEE Journal of Emerg. and Sel. Topics in Power Electr.*, vol. 10, no. 2, pp. 1925–1934, 2022.

[4] M. J. Corley and R. D. Lorenz, "Rotor position and velocity estimation for a salient-pole permanent magnet synchronous machine at standstill and high speeds," *IEEE Trans. Ind. Appl.*, vol. 34, no. 4, 1998.

[5] V. Manzolini and S. Bolognani, "On the rotor position self-sensing capability of reluctance and IPM synchronous motors," *IEEE Trans. Ind. Electron.*, vol. 56, no. 4, pp. 3755–3766, 2020.

[6] M. Berto, P. G. Carlet, V. Manzolini, and L. Alberti, "An effective ellipse fitting technique of the current response locus to rotating HF voltage injection in IPMSM for sensorless rotor position estimation," in *IECON 2018 - 44th Ann. Conf. of the IEEE Ind. Electron. Soc.*, 2018.

[7] F. Toso, M. Berto, L. Alberti, and F. Marcuzzi, "Efficient QR updating factorization for sensorless synchronous motor drive based on high frequency voltage injection," *IEEE Trans. Ind. Electron.*, vol. 67, no. 12, pp. 10 213–10 222, 2020.

[8] S. Kim, J. Im, E. Song, and R. Kim, "A new rotor position estimation method of IPMSM using all-pass filter on high-frequency rotating voltage signal injection," *IEEE Trans. Ind. Electron.*, vol. 63, no. 10, pp. 6499–6509, 2016.

[9] A. Yousefi-Talouki, P. Pescetto, and G. Pellegrino, "Sensorless direct flux vector control of synchronous reluctance motors including standstill, mtpa, and flux weakening," *IEEE Trans. Ind. Appl.*, vol. 53, no. 4, pp. 3598–3608, 2017.

[10] J. Jang, S. Sul, J. Ha, K. Ide, and M. Sawamura, "Sensorless drive of surface-mounted permanent-magnet motor by high-frequency signal injection based on magnetic saliency," *IEEE Trans. Ind. Appl.*, vol. 39, no. 4, pp. 1031–1039, 2003.

[11] M. W. Degner and R. D. Lorenz, "Using multiple saliencies for the estimation of flux, position, and velocity in AC machines," *IEEE Trans. Ind. Appl.*, vol. 34, no. 5, pp. 1097–1104, 1998.

[12] V. Manzolini, M. Morandin, and S. Bolognani, "The crowded axis of the frequency: Optimal pole/zero allocation for a full speed sensorless synchronous motor drives," in *2016 IEEE Energy Convers. Congr. and Expo. (ECCE)*, 2016, pp. 1–8.

[13] L. Ortombina, D. Pasqualotto, F. Tinazzi, and M. Zigliotto, "Magnetic model identification of synchronous motors considering speed and load transients," *IEEE Trans. Ind. Appl.*, vol. 56, no. 5, pp. 4945–4954, 2020.

[14] M. Berto, L. Alberti, V. Manzolini, and S. Bolognani, "Computation of self-sensing capabilities of synchronous machines for rotating high frequency voltage injection sensorless control," *IEEE Trans. Ind. Electron.*, vol. 69, no. 4, pp. 3324–3333, 2022.

[15] Y. Kwon, J. Lee, and S. Sul, "Extending operational limit of IPMSM in signal-injection sensorless control by manipulation of convergence point," *IEEE Trans. Ind. Appl.*, vol. 55, no. 2, pp. 1574–1586, 2019.

[16] W. Zine, L. Idkhajine, L. Kobylanski, E. Monmasson, P. Chauvenet, A. Bruyere, and B. Condamin, "Compensation of cross-saturation effects on ipmsm sensorless control - application to electric vehicle," in *42nd Annual Conf. of the IEEE Ind. Electron. Soc.*, 2016, pp. 6675–6680.

[17] Y. Yoon, S. Sul, S. Morimoto, and K. Ide, "High-bandwidth sensorless algorithm for AC machines based on square-wave-type voltage injection," *IEEE Trans. Ind. Appl.*, vol. 47, no. 3, pp. 1361–1370, 2011.

[18] S. Yang, S. Yang, and J. Hui Hu, "Design consideration on the square-wave voltage injection for sensorless drive of interior permanent-magnet machines," *IEEE Trans. Ind. Electron.*, vol. 64, no. 1, pp. 159–168, 2017.

[19] G. Wang, D. Xiao, G. Zhang, C. Li, X. Zhang, and D. Xu, "Sensorless control scheme of IPMSMs using HF orthogonal square-wave voltage injection into a stationary reference frame," *IEEE Trans. Power Electron.*, vol. 34, no. 3, pp. 2573–2584, 2019.

[20] L. Ortombina, M. Berto, and L. Alberti, "Synchronous motor sensorless drives based on rotating signal injection and direct ellipse estimation," in *2021 International Conf. on Optim. of Elect. and Elect. Equip. (OPTIM)*, 2021, pp. 413–419.

[21] N. Bedetti, S. Calligaro, and R. Petrella, "Self-commissioning of inverter dead-time compensation by multiple linear regression based on a physical model," *IEEE Trans. Ind. Appl.*, vol. 51, no. 5, pp. 3954–3964, 2015.

Ludovico Ortombina (M' 19) received the M.S and Ph.D. degree in Mechatronics Engineering from the University of Padova, Italy, in 2015 and 2019, respectively. Since August 2020, he is a Researcher with the Department of Industrial Engineering, University of Padova. His research interests include parameter estimation techniques for synchronous motors, sensorless controls and predictive control.

Matteo Berto was born in Venice, Italy. He received the B.S., M.S., and Ph.D. degrees in Electrical Engineering from the University of Padova, Italy, in 2016, 2018, and 2022, respectively. He is currently a Motor Controls Engineer working for BorgWarner Systems Eng. GmbH, Nuremberg, Germany. His main research interests include positon sensing and sensorless control for ac motors.

Luigi Alberti (SM'20) received the Laurea and the Ph.D. degrees in electrical engineering from the University of Padova, Padova, Italy, in 2005 and 2009, respectively. From 2009 to 2012, he was a Research Associate at the University of Padova. In 2012, he moved to the Faculty of Science and Technology, Free University of Bozen-Bolzano, Italy, to start research and educational activities in the field of electrical engineering and electrical machines. He is currently an Associate Professor with the Department of Industrial Engineering, University of Padova, working on design, analysis, and control of electric machines and drives, with particular interest in renewable energies and more electric vehicles.